4th International Conference on the Durability of Concrete Structures
24–26 July 2014
Purdue University, West Lafayette, IN, USA

Research on Microscopic Pore Structure and Permeability of Air-Entrained Fly–Ash Concrete Subjected to Freezing and Thawing Action

Zhuo Zhao
School of Civil Engineering and Architecture, Ningbo University of Technology

Dawang Li, Feng Xing, and Ningxu Han
College of Civil Engineering, Shenzhen University
Guangdong Provincial Key Laboratory of Durability for Marine Civil Engineering

Dongwei Wang
School of Civil Engineering, Zhengzhou University

ABSTRACT

In this paper, rapid freezing and thawing test of air-entrained fly–ash concrete was carried out. Gas adsorption of concrete pores, mass loss, dynamic elastic modulus, and chloride diffusion coefficient of concrete after different freezing and thawing cycles was tested; scanning electron image was used to study the microscopic pore structure of the specimens. Results show that after certain freezing and thawing cycles, microscopic pores of the sample had a brittle failure, which results in sudden changes of cumulative desorption pore volume and cumulative desorption surface area obtained by Barrett, Joyner, and Halenda method. It was found that the variation of maximum cumulative desorption surface area is in good agreement with that of mass loss rate and chloride diffusion coefficient. At different stages of freezing and thawing, rate of mass loss shows a linear relationship with maximum cumulative desorption pore volume and maximum cumulative desorption surface area. In the range of freezing and thawing cycle between 0 and 150, chloride diffusion coefficient demonstrates a linear relationship with maximum cumulative desorption pore volume and maximum cumulative desorption surface area; in the range of freezing and thawing cycle between 200 and 300, this relationship becomes nonlinear.

1. INTRODUCTION

Under a saturated state, concrete may be deteriorated under the effect of rigorous freezing and thawing temperatures, which is a physical process and is named the freezing and thawing damage. The frost resistance is usually used to demonstrate the resistance of concrete to the freezing and thawing effect. Adding appropriate air-entraining agent in concretes is commonly used in industry to improve the frost resistance of concrete.

Due to the effect of freezing and thawing, the microscopic structure of concrete will be changed, resulting in the variation of the concrete performances, such as chloride diffusion coefficient, dynamic elastic modulus, strength, mass loss rate, and so on. Theoretical and experimental researches on the influence of freezing and thawing damage on the macroscopic physical, mechanical, and durability performance of concrete have been carried out (Li, Sun, & Jiang, 2009; Saito, Tanaka, & Ishimori, 2001; Zou, Zhao, & Liang, 2008). As a result, standards concerning the test method and design control index for frost resistance of concrete have been proposed (China Academy of Building Research, 2009; Tsinghua University, 2008).

To certain extent, the relationship between the microscopic structure and performance of concrete has been revealed by means of morphology, porosity, pore size distribution, air content, and air bubble spacing (Chen, Yang, Zhou, et al., 2011; Nokken & Hooton, 2008; Zhang, Wang, & Wang, 2010; Zhao, Wei, & Huang, 2002). However, the impact of variation of microstructure on the frost performance of concrete needs to be further profoundly investigated, due to the nonuniformity and complexity of the concrete microstructure.

In this paper, rapid freezing and thawing test of air-entrained fly–ash concrete was carried out. With the help of the scanning electron image (SEI) and the gas adsorption analysis, properties such as the mass loss, dynamic elastic modulus, and chloride diffusion coefficient were studied after various freezing and thawing cycles. The relationship between microscopic structure and performance of concrete was the major concern regarding to the frost behavior among the durability issues.

2. EXPERIMENTAL STUDIES

2.1 Test materials

Cement: P·O 42.5 ordinary Portland cement, the specific surface area is 367 m^2/kg. Fine aggregate: natural river sand, its fineness modulus is 2.3 and apparent density is 2691 kg/m^3. Coarse aggregate: 5–20 mm graded gravel and the apparent density is 2708 kg/m^3. Fly ash: second level of F class and its fineness is 20.1%. Admixtures: HT-HPC liquid state polycarboxylate super-plasticizer and its water reduction rate is 25%, YF-HQ paste state air-entraining agent.

2.2 Concrete mix proportion

According to test code for hydraulic concrete (SL352-2006; China Institute of Water Resources Hydropower Research, 2006), specification for mix proportion design of ordinary concrete (JGJ55-2011; China Academy of Building Research, 2011), water–cementitious materials ratio, sand, crushed stone aggregate, amount of cementitious materials, sand ratio, admixtures, water consumption, and so on, was preliminary selected. The proportion of adopted concrete mix is shown in Table 1.

Table 1. Mix proportion of concrete (kg/m^3).

Cement	209
Sand	770
Crushed stone 5–20 mm	1207
Water	120
Fly ash	52
Super plasticizer	2.4795
Air-entraining agent	0.0261
Slump (mm)	65
Air content (%)	4.75

2.3 Experiments

Details of the tests carried out are shown in Table 2.

Table 2. Test items of concrete.

Test	Number of Specimen	Dimension of Specimen	Test Parameter
Freezing and thawing	6	100 mm × 100 mm × 400 mm	Relative dynamic elastic modulus, rate of mass loss
Chloride resistance	6	100 mm × 50 mm	Diffusion coefficient of chloride
Microstructure	6	100 mm × 100 mm × 100 mm	Morphology and pore structure

The relative dynamic elastic modulus and mass loss rate were determined by rapid freezing and thawing method according to GBT 50082-2009 (China Academy of Building Research, 2009).

The diffusion coefficient of chloride under different freezing and thawing cycles was determined according to JTG/T B07-01-2006 (Changsha University of Science and Technology & Tsinghua University, 2006).

After different freezing and thawing cycles, SEI and gas adsorption analysis were used to observe the change of microscopic structure of concrete.

3. EXPERIMENTAL RESULTS AND DISCUSSIONS

3.1 Experimental results

Mass and dynamic elastic modulus obtained after different freezing and thawing cycles are shown in Table 3.

Chloride diffusion coefficient obtained after different freezing and thawing cycles is shown in Table 4.

Table 3. Mass and dynamic elastic modulus after different freezing and thawing cycles.

Freezing and Thawing Cycle	Mass (g)	Dynamic Elastic Modulus (MPa)
0	9709.66	41091
25	9707.99	38743
50	9710.15	38495
75	9704.80	38513
100	9702.96	38201
125	9699.26	38218
150	9696.82	38127
175	9691.67	38167
200	9674.26	38193
225	9657.85	38080
250	9644.13	37880
275	9643.28	36541
300	9637.50	36071

Table 4. Chloride diffusion coefficient after different freezing and thawing cycles.

Freezing and Thawing Cycle	Chloride Diffusion Coefficient (10^{-12} m^2/s)
0	13.1
25	13.2
50	13.7
75	14.8
100	15.6
125	15.7
150	15.9
175	15.8
200	15.9
225	16.4
250	16.6
275	17.3
300	18.9

SEI micrograph after various freezing and thawing cycles is shown in Figure 1.

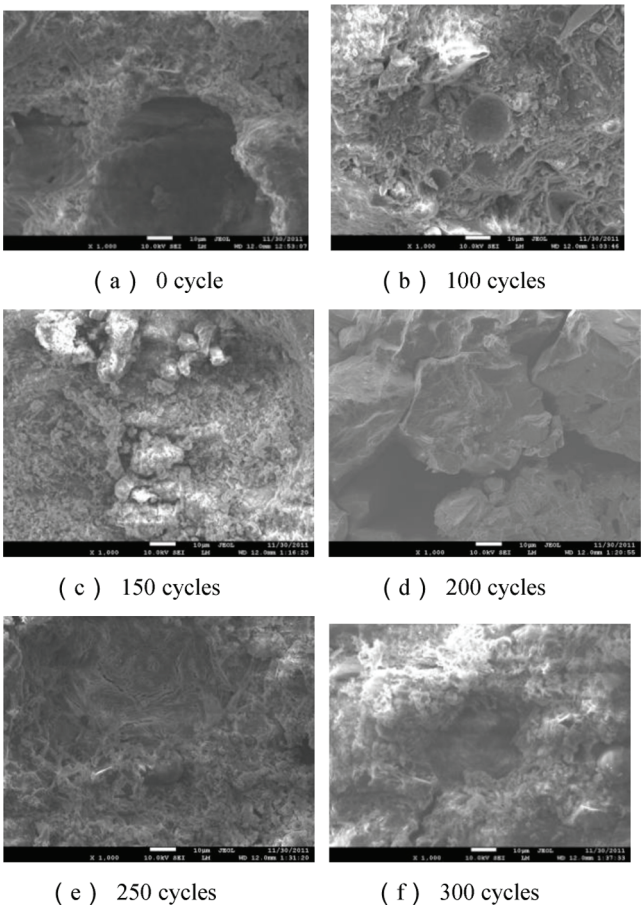

Figure 1. SEM micrograph of concrete after different freezing and thawing cycles (1000×).

Characteristics of pores determined by means of gas adsorption analysis after different freezing and thawing cycles are shown in Table 5.

Table 5. Pore characteristics after different freezing and thawing cycles.

Freezing and Thawing Cycle	Maximum Cumulative Desorption Pore Volume (cc/g)	Maximum Cumulative Desorption Surface Area (m^2/g)	Average Pore Radius (Å)
0	2.64E-02	1.73E+01	6.71E+01
100	4.85E-02	2.90E+01	5.87E+01
150	6.77E-02	3.01E+01	6.28E+01
200	4.38E-02	2.02E+01	6.02E+01
250	6.94E-02	3.11E+01	5.93E+01
300	6.64E-02	3.36E+01	6.80E+01

3.2 Discussions

3.2.1 Microscopic structure

As shown in Figure 1, the microscopic pore structure of concrete changed subsequently with the increase of freezing and thawing circles. Figure 1(b) shows that after 100 freezing and thawing cycles, the microporosity increased and larger pores were connected, which caused the formation of a layered conglomeration state. Figure 1(c) shows that after 150 cycles, plastic particles were produced with a continuous increase of micro pores. Figure 1(d) shows that after 200 cycles, there was an apparent brittle failure of the pore structure, large pores were connected, hydrated cement paste was divided into pieces and overall compactness of concrete declined substantially. Figure 1(e) shows that after 250 cycles, there were numerous pores in the structure and those had relatively larger diameter were connected, which formed a stacked structure with distributed layers. Figure 1(f) shows that after 300 cycles, minerals were covered by concentrated pores and numerous amounts of debris, formed under the effect of freezing and thawing, accumulated in the structure.

In summary, under the effect of freezing and thawing, concrete pores with relatively smaller dimension developed continuously and increased in size, which led to the brittle failure of the structure. Meanwhile, micro pores were also generated continuously. With the increase in the number of freezing and thawing cycle, defects in the concrete developed and a large number of debris produced.

3.2.2 Relationship between Barrett, Joyner, and Halenda method (BJH) cumulative desorption pore volume with rate of mass loss and chloride diffusion coefficient

The relationship between pore radius and cumulative desorption pore volume, calculated from the basis of BJH method, after different freezing and thawing cycles is shown in Figure 2.

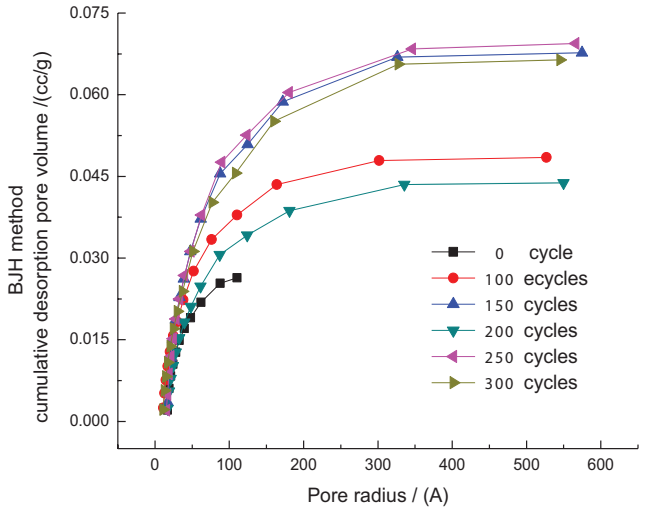

Figure 2. Relationship between cumulative desorption pore volume and pore radius.

As shown in Figure 2, the cumulative desorption pore volume decreased significantly after 200 freezing and thawing cycles. This should be due to the brittle failure

of concrete pore structure between the 150 and 200 freezing and thawing cycles, as shown in Figure 1(d). At this stage, grout matrix was divided into pieces with relatively bigger pores (>100 nm), whose size is beyond the testing range of the gas adsorption method (China Academy of Sciences, Institute of Process Engineering, Center of Physical and Chemical Analysis and Test in Beijing, 2008). Therefore, the volume of these pores could not be measured. Under the effect of freezing and thawing, micro pores were generated continuously on the produced new pieces and the pore volume presented a trend of gradually increase.

The relationship between maximum cumulative desorption pore volume and mass loss rate after different freezing and thawing cycles is shown in Figure 3, and that between maximum cumulative desorption pore volume and chloride diffusion coefficient is shown in Figure 4.

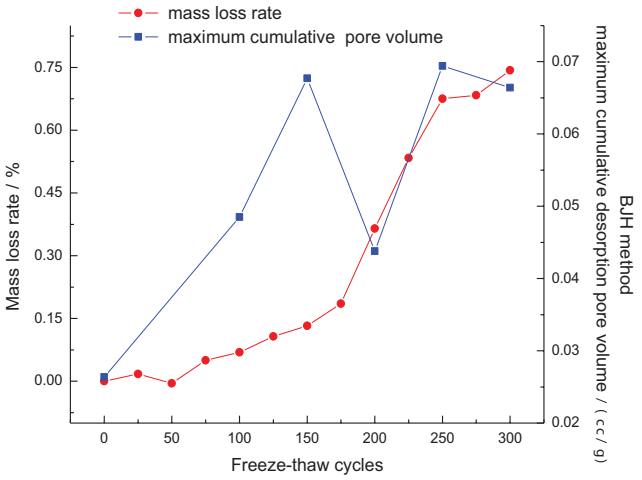

Figure 3. Relationship between maximum cumulative desorption pore volume and rate of mass loss.

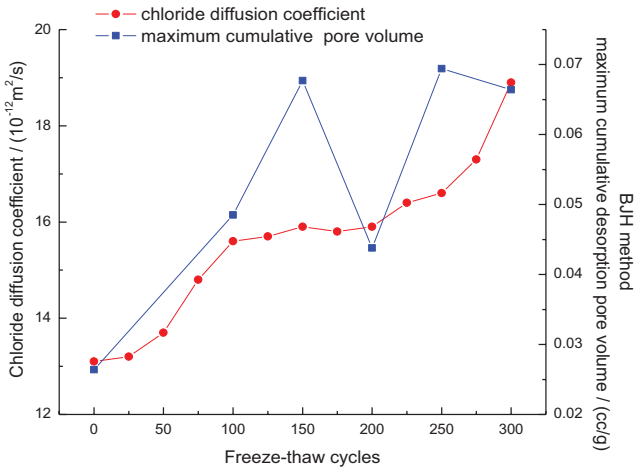

Figure 4. Relationship between maximum cumulative and diffusion coefficient of chloride.

Figure 3 shows that the mass loss rate increased with the number of freezing and thawing cycles. The variation of mass loss rate has an apparent inflection after 175 freezing and thawing cycles, which corresponds to the brittle failure of pore structure and the change of maximum cumulative desorption pore volume. Both the variation of maximum cumulative desorption pore volume and mass loss rate present inflections at the 250 freezing and thawing cycles; the maximum cumulative desorption pore volume is slightly lower, and mass loss rate shows a relatively modest increase.

As shown in Figure 4, the chloride diffusion coefficient generally increased with the number of freezing and thawing cycle. An inflection of chloride diffusion coefficient appears at the 200 freezing and thawing cycles, which is corresponding to the brittle failure of pore structure and the change of maximum cumulative desorption pore volume. Both the variation of maximum cumulative desorption pore volume and chloride diffusion coefficient present inflections at 250 freezing and thawing cycles; the maximum cumulative desorption pore volume is slightly lower, and chloride diffusion coefficient presents a much obvious growth.

Considering the brittle failure of concrete microscopic pore structure, the freezing and thawing process can be divided into two stages, namely, 0–150 cycles of freezing and thawing stage and 200–300 cycles of freezing and thawing stage.

The relationship between maximum cumulative desorption pore volume and mass loss rate at different freezing and thawing stages is obtained by linear regression and is shown in Figure 5. The relationship between maximum cumulative desorption pore volume and chloride diffusion coefficient at different freezing and thawing stage is shown in Figure 6.

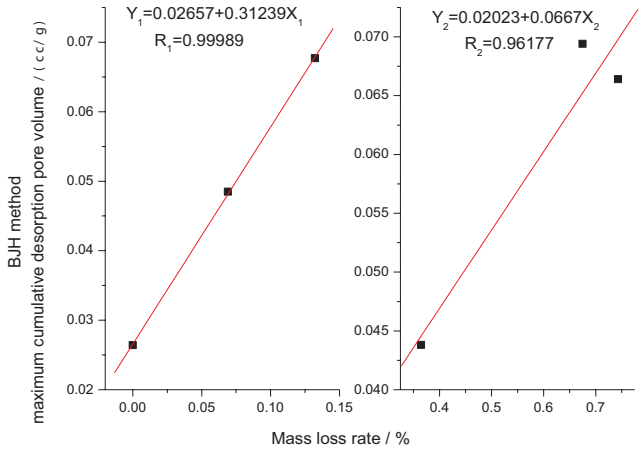

Figure 5. Regression relationship between the maximum cumulative desorption pore volume and mass loss rate.

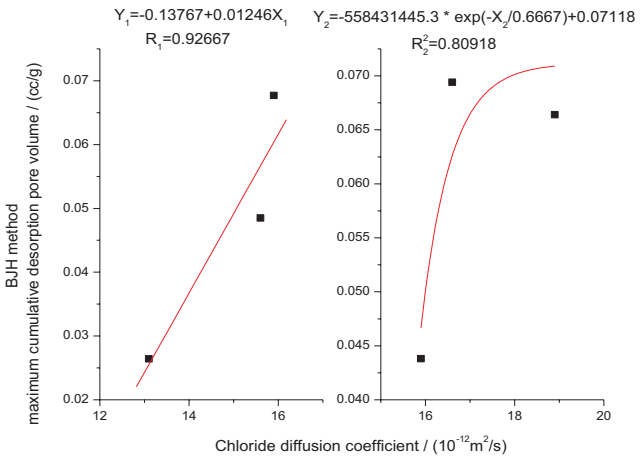

Figure 6. Regression relationship between the maximum cumulative desorption pore volume and chloride diffusion coefficient.

As shown in Figure 5, at the two stages, the mass loss rate has a good linear relationship with the maximum cumulative desorption pore volume.

As shown in Figure 6, at the stage of 0–150 freezing and thawing cycles, chloride diffusion coefficient is approximated linear related to the maximum cumulative desorption pore volume. While, at the stage of 200–300 cycles, the relationship is missing, this may be due to the split-up of the grout matrix after 200 freezing and thawing cycles. The development of microcrack and formation of relatively larger pores in the matrix lead to the complex variation of chloride diffusion coefficient.

3.2.3 Relationship between BJH cumulative desorption surface area with mass loss rate and chloride diffusion coefficient

The relationship between pore radius and cumulative desorption surface area, calculated from the basis of the BJH results, is shown in Figure 7.

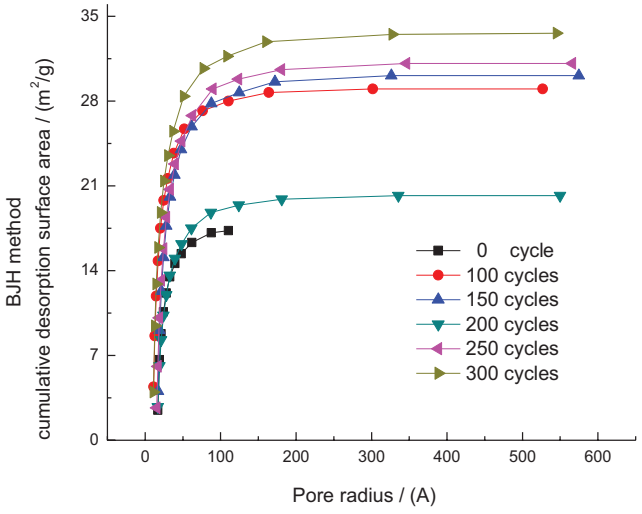

Figure 7. Relationship between cumulative desorption surface area and pore radius.

As shown in Figure 7, the development of cumulative desorption surface area is similar to that of cumulative desorption pore volume.

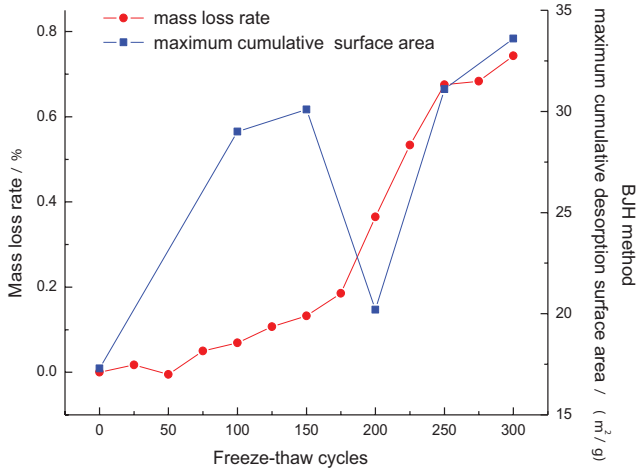

Figure 8. Relationship between maximum cumulative desorption surface area and mass loss rate.

Figure 8 shows the relationship between the mass loss rate and the maximum cumulative desorption surface area during the freezing and thawing circles. It is similar to that between the mass loss rate and the maximum cumulative desorption pore volume, as shown in Figure 3. Both the maximum cumulative desorption surface area and mass loss rate curves increased with the freezing and thawing cycles and have an obvious inflection after 250 cycles.

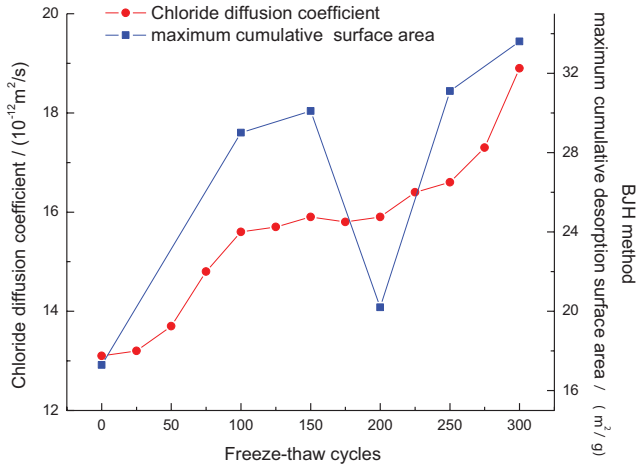

Figure 9. Relationship between maximum cumulative desorption surface area and the chloride diffusion coefficient.

Figure 9 shows the relationship between the chloride diffusion coefficient and the maximum cumulative desorption surface area. Compared with Figure 8, it is found that the chloride diffusion coefficient fits the maximum cumulative surface area in a better degree than the mass loss rate. Before 100 freezing and thawing

cycles, the chloride diffusion coefficient increases correspondingly with the maximum cumulative surface area. At the 100 cycles, the two curves show an apparent inflection and turn to a modest increase stage after that. The value for the chloride diffusion coefficient of samples, affected by 200 freezing and thawing circles, shows an obvious increase. This corresponds to the apparent variation in the curve of the maximum cumulative desorption surface area. Both of the two parameters have another inflection point at the 250 circles and increase in the subsequent stage.

The relationships between the maximum cumulative desorption surface area and the mass loss rate at stages of 0–150 and 200–300 freezing and thawing circles are obtained by means of linear regression and are shown in Figure 10. The two parameters have good linear relationships in these two stages.

The relationships between maximum cumulative desorption surface area and chloride diffusion coefficient at 0–150 and 200–300 freezing and thawing circles are shown in Figure 11.

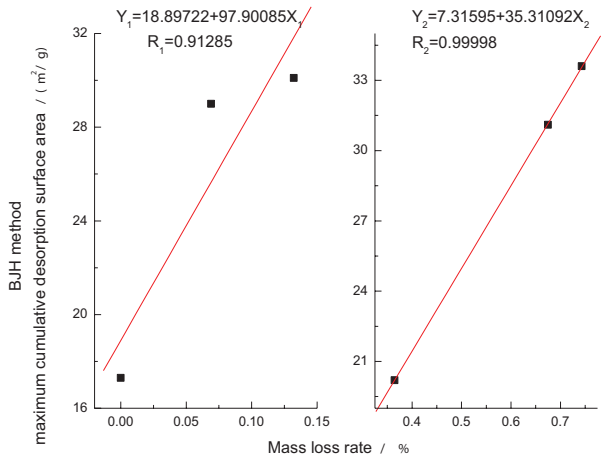

Figure 10. Regression relationship between the maximum cumulative desorption surface area and the mass loss rate.

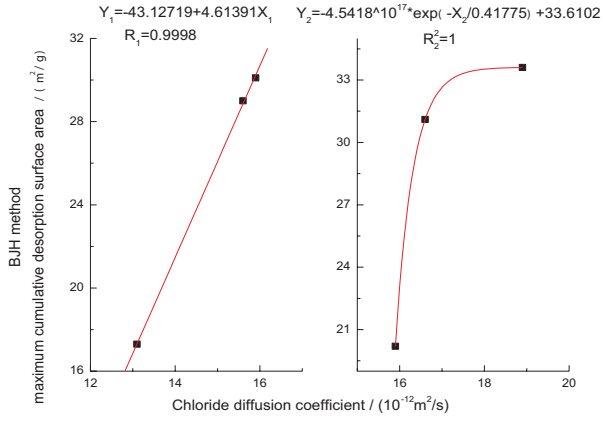

Figure 11. Regression relationship between the maximum cumulative desorption surface area and the chloride diffusion coefficient.

At stage of 0–150 freezing and thawing cycles, the chloride diffusion coefficient has a good linear relationship with the maximum cumulative desorption surface area; at stage of 200–300 cycles, it becomes nonlinear.

3.2.4 Average pore radius

It can be seen through comparison of average pore radius after different freezing and thawing cycles that the average pore radius of concrete varied slightly with the cycles of freezing and thawing. This should be due to the variation of the pore structure. New micro pores were generated, and meanwhile, existed pores are connected and increased in size. Part of the bigger pores is beyond the testing range of the gas adsorption method.

4. CONCLUSIONS

(1) With the increase in the number of freezing and thawing cycles, the chloride diffusion coefficient and mass loss rate increased, while the dynamic elastic modulus decreased.

(2) After about 200 freezing and thawing cycles, concrete microscopic pore structure experienced a brittle failure, which resulted in a sudden change of cumulative desorption pore volume and cumulative desorption surface area. This let to variation of chloride diffusion coefficient and mass loss rate of the concrete.

(3) After different freezing and thawing cycles, the variations of the maximum cumulative desorption pore volume and the maximum cumulative desorption surface area are in good agreements with those of the mass loss rate and the chloride diffusion coefficient. Compared with the maximum cumulative desorption pore volume, the maximum cumulative desorption surface area presents a better correlation with that of the chloride diffusion coefficient and the mass loss rate.

(4) At two different stages of freezing and thawing cycles, the mass loss rate has good linear correlation relationships with the maximum cumulative desorption pore volume and the maximum cumulative desorption surface area.

(5) At the stage of 0–150 freezing and thawing cycles, the chloride diffusion coefficient presents a relationship with the maximum cumulative desorption pore volume and the maximum cumulative desorption surface area. At the stage of 200–300 freezing and thawing cycles, the linear relationship between the parameters is missing.

ACKNOWLEDGMENTS

The authors appreciate the financial supports by the National Natural Science Foundation of China (51078334, 51278303) and Henan Province Communication and Transport Department (2012D10).

REFERENCES

Changsha University of Science and Technology & Tsinghua University. (2006). *Specification for deterioration prevention of highway concrete structures (JTG/T B07-01-2006)*. Beijing: China Communications Press [in Chinese].

Chen, X., Yang, H., Zhou, S. et al. (2011). Research on concrete freezing and thawing durability and characteristic parameters of bubbles. *Journal of Building Materials [in Chinese], 14*(2), 257–262.

China Academy of Building Research. (2009). *Standard for test methods of long-term performance and durability of ordinary concrete (GB/T50082-2009).* Beijing: China Architecture & Building Press [in Chinese].

China Academy of Building Research. (2011). *Specification for mix proportion design of ordinary concrete (JGJ55-2011)*. Beijing: China Architecture & Building Press [in Chinese].

China Academy of Sciences, Institute of Process Engineering, Center of Physical and Chemical Analysis and Test in Beijing. (2008). *Pore size distribution and porosity of solid materials by mercury porosimetry and gas adsorption. Part 2: Analysis of mesopores and macropores by gas adsorption (GB/T21650. 2--2008/IS0 15901-2: 2006)*. Beijing: China Standards Press [in Chinese].

China Institute of Water Resources Hydropower Research. (2006). *Test code for hydraulic concrete (SL352-2006).* Beijing: China Water Power Press [in Chinese].

Li, W., Sun, W., & Jiang, J. (2009). Review on damage and deterioration of concrete sbujected to the coupling effect of fatigue load and environmental actions. *Journal of the Chinese Ceramic Society, 37*(12), 2142–2149.

Nokken, M. R., & Hooton, R. D. (2008). Using pore parameters to estimate permeability or conductivity of concrete. *Materials and Structures, 41*(1), 1–16.

Saito, M., Tanaka, S., & Ishimori, H. (2001). Chloride permeability of lightweight concretes subjected to freeze–thaw cycles. *Zairyo/Journal of the Society of Materials Science* [in Japanese]*, 50*(2), 180–186.

Tsinghua University. (2008). *Code for durability design of concrete structures (GB/T50476-2008).* Beijing: China Architecture & Building Press [in Chinese].

Zhang, F., Wang, H., & Wang, Q. (2010). Study on effects of mineral admixture and air-entraining agent on the pore structure and performance of concrete. *Journal of Hydroelectric Engineering* [in Chinese]*, 29*(1), 180–185.

Zhao, X., Wei, J., & Huang, Y. (2002). Relationship betwen pore structure change of concrete and its frost durability degradation. *Journal of Wuhan University of Science and Technology* [in Chinese]*, 24*(12), 14–17.

Zou, C., Zhao, J., & Liang, F. (2008). Degradation of mechanical properties of concrete caused by freeze–thaw action. *Journal of Building Structures* [in Chinese]*, 29*(1), 117–138.